
A Neutron Temporal Diagnostic for High-Yield DT Cryogenic Implosions on OMEGA

Introduction

The temporal history of the neutron production in inertial confinement fusion (ICF) experiments¹ is an important diagnostic signature. In ICF experiments, shells filled with deuterium (D₂) or a deuterium–tritium (DT) mixture are compressed by either direct laser illumination,² soft x-ray radiation in a laser-heated hohlraum,³ or strong magnetic fields⁴ to conditions under which thermonuclear fusion occurs. The temporal width of the neutron signal is usually of the order of 100 ps. Experimental signatures from the temporal history of the neutron production are the rising edge of the measured neutron rate, which is influenced by the shock transit through the capsule;⁵ the peak of the neutron rate (bang time),⁶ a measure of the energy absorbed in the imploding shell; and the trailing edge of the neutron rate that encodes information about material mixing during the stagnation phase of the implosion.⁷

Time-resolved neutron measurements on ICF experiments generally use either a scintillator to convert the neutron energy into visible light⁸ or chemical-vapor–deposition (CVD) diamond detectors,⁹ which convert the neutron energy directly into an electrical charge. The light from the scintillator is either converted into an electrical signal using a fast photomultiplier tube (PMT) or recorded on a fast optical streak camera.^{10,11} The PMT or CVD-based neutron bang-time diagnostics^{12–16} do not have the temporal resolution to resolve the details of the neutron pulse; they measure solely the neutron bang time. Only the streak-camera–based neutron temporal diagnostics (NTD’s)^{10,11} are capable of resolving the details of the neutron temporal history.

High-performance, layered cryogenic DT implosions¹⁷ on the OMEGA laser¹⁸ at the Laboratory for Laser Energetics (LLE) present a particular challenge in measuring the neutron history because of the high-DT neutron yields ($\sim 5 \times 10^{13}$) and a short neutron-production width (of the order of ~ 50 ps). The size of the cryogenic target shroud system¹¹ prevents the placement of the scintillator of the NTD system sufficiently close to the target to minimize Doppler broadening of the neutron pulse, which severely compromises the time resolution of the NTD.¹⁰ A dedicated cryogenic-compatible neutron tempo-

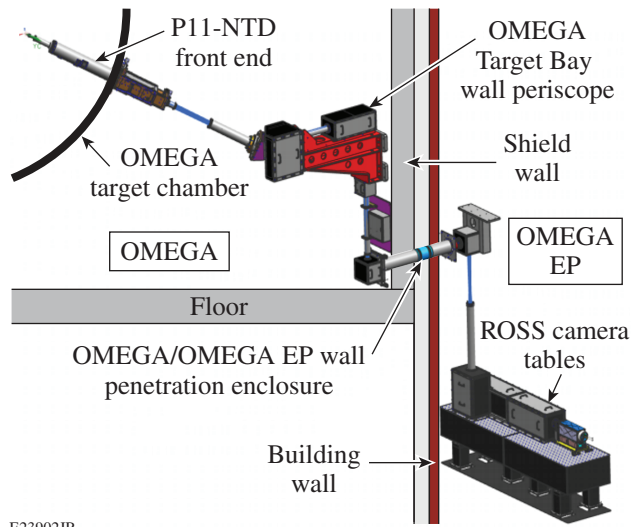
ral diagnostic (cryoNTD) was developed at LLE to provide high-resolution neutron-emission measurements for D₂-filled cryogenic implosions,¹¹ but the placement of the streak camera close to the target chamber prevents recording data at high-DT yields because of the excessive neutron background. This article describes the setup of a new NTD system at LLE designed for high-performance, layered DT cryogenic implosions mounted in port P11 of the OMEGA target chamber (P11-NTD). The next section presents the setup of this system. The scintillator can be inserted as close as 9 cm from the target in cryogenic experiments without interfering with the cryogenic target systems. The streak camera is placed in a well-shielded location >10 m from the target, with an ~ 16 -m-long optical relay system transporting the optical signal from the scintillator to the streak camera. The remaining sections report on the performance of the shielding setup, present the temporal impulse-response calibration procedure of the P11-NTD system, and analyze the first experimental results.

Setup of the Detector System

A CAD drawing of the P11-NTD system setup is shown in Fig. 145.34. The front-end scintillator insertion mechanism is a re-entrant into the OMEGA target chamber. A 6-mm-diam, 1-mm-thick plastic scintillator (Bicron BC422) (Ref. 19) is placed in a tungsten-alloy–shielded nose cone,¹⁰ which can be inserted between 2 cm and 25 cm from the target. The first section of the optical relay system is housed inside the front end. The second section of the optical relay, the Target Bay wall periscope, is mounted to the OMEGA Target Bay shield wall. The optical path then leads from the OMEGA building into the OMEGA EP plenum, where the Rochester Optical Streak System (ROSS)²⁰ camera is mounted on an optical table.

1. Neutron Shielding

Historically, the streak camera of an NTD system has been placed close to the target chamber to minimize the length of the optical relay system.^{10,11} This approach works very well for moderate yields ($<1 \times 10^{13}$ neutrons) but does not provide enough shielding to suppress the backgrounds for the high-DT neutron yields (up to 5×10^{13}) produced in cryogenic DT



E23902JR

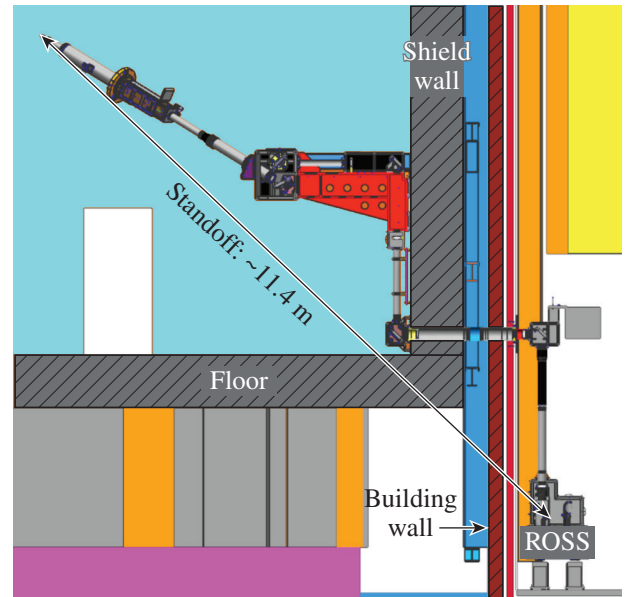
Figure 145.34

A CAD drawing of the P11-NTD (neutron-temporal-diagnostic) detector system integrated into the Omega Laser Facility. A front-end system re-entrant into the target chamber positions the scintillator distances between 2 to 25 cm from the target. An optical relay partially housed in the Target Bay wall periscope structure transports the scintillator light through a penetration in the OMEGA shield wall to a ROSS streak camera in the OMEGA EP plenum.

implosions on OMEGA.¹⁷ To improve the shielding, the streak camera for the P11-NTD was placed behind the primary shield wall of the OMEGA target area in the OMEGA EP plenum (see Fig. 145.35). This location provides a standoff distance to the target of ~ 11.4 m, with ~ 1.7 m of concrete in the direct line of sight, which penetrates the OMEGA Target Bay floor, the OMEGA Target Bay retaining wall, and a brick facing wall. It is well known that the performance of a neutron shielding system depends not only on the shielding thickness in the direct line of sight, but also on the number and area of openings such as doors and holes in the shielded volume, which allow scattered neutrons to escape the target area.²¹ Since there is a large ~ 1 -m-diam hole under the target chamber, an ~ 1 -m-diam beam tube that carries the OMEGA EP laser pulse from OMEGA EP to OMEGA for joint experiments,²² and a number of doors into the room under the target area, the performance of this shielding will be worse than a simple estimate using the thickness of the direct line of sight would indicate.

2. Optical System

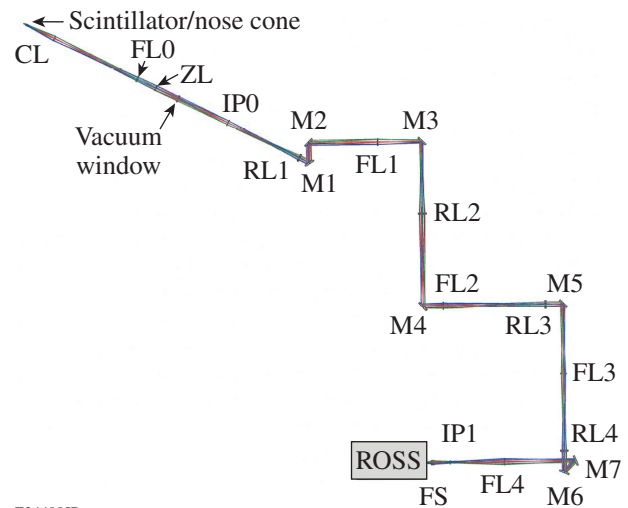
With the location of the streak camera in a separate building, a relatively complex 16.2-m-long optical path had to be designed. The light collection and transfer system (Fig. 145.36) transports the light from the scintillator to the input plane of ROSS. A fast three-element $f/2$ lens system collects (CL) the light from the scintillator. A zoom (ZL) and field lens (FL0) relay the light through the vacuum window to an intermediate image plane (IP0). A four-stage optical relay, each consisting of an achromatic relay lens (RL1–4) and a field lens (FL1–4), transports the light from the first intermediate image using seven mirrors (M1–M7) to a second image plane (IP1). A three-element focus lens system (FS) focuses the light onto the slit of the streak camera.



E23905JR

Figure 145.35

A CAD drawing of the P11-NTD shielding setup. The ROSS streak camera is placed 11.4 m from the target. The 60-cm-thick OMEGA target area floor and 80-cm-thick Target Bay shield wall provide most of the neutron shielding.



E24498JR

Figure 145.36

A drawing of the optical layout of the relay optics. A fast three-element $f/2$ lens system collects (CL) the light from the scintillator. A zoom (ZL) and field lens (FL0) relay the light through the vacuum window to an intermediate image plane (IP0). A four-stage optical relay, each consisting of an achromatic relay lens (RL1–4) and a field lens (FL1–4), transports the light from the first intermediate image using seven mirrors (M1–M7) to a second image plane (IP1). A three-element focus lens system (FS) focuses the light onto the slit of the streak camera.

zoom lens and a field lens relays the light from the scintillator to an intermediate image plane outside the target chamber. The location of the zoom lens is adjusted to keep the location of the intermediate image plane fixed. A four-stage optical relay, each consisting of an achromatic relay lens and a field lens, transports the light from the first intermediate image plane to an image plane close to the ROSS camera on the optical table in the OMEGA EP building. A three-element achromatic $f/4$ lens system focuses the light from the last image plane onto the photocathode of the ROSS. Since the optical path is not a straight line, seven turning mirrors were required to relay the light from the target chamber through the OMEGA shield wall into the OMEGA EP building. High-quality broadband antireflective (AR) coatings were used on the lenses with a typical loss of $\sim 0.3\%$ per surface, at normal incidence and dielectric high-reflective (HR) coatings were used on the mirrors with a reflectivity of $>98.5\%$ over the full spectral width of the scintillator emission from ~ 350 nm to 450 nm (Ref. 19). The total transmission of the system was estimated to be $\sim 55\%$, with $\sim 20\%$ losses in the lens material, $\sim 25\%$ in the AR coatings as a result of the incident angular range, and $\sim 10\%$ in the HR coatings.

Even though the optical system is corrected for chromatic aberrations, the chromatic velocity dispersion caused by the change in index of refraction with wavelength will introduce a broadening of the impulse response. Using published values for the index of refraction²³ of the glasses used in the optical system, this effect was estimated for the optical ray passing through the center of all optics to broaden the full width at half maximum (FWHM) of the instrument response by ~ 8 ps given the spectrum of the scintillator light emission. This value should be considered an upper limit since most of the light passes through thinner glass than the center ray and consequently experiences less chromatic velocity dispersion.

In addition to the signal from the scintillator, light from the OMEGA fiducial system is delivered via an optical fiber and imaged onto the streak camera using an optical system internal to the ROSS camera. The OMEGA fiducial consists of a series of eight pulses spaced 548 ps apart and is amplified separately from the main laser pulse, split, and distributed to various diagnostic instruments for precision timing. This fiducial is also recorded on the P510 ultraviolet streak camera,²⁴ which measures the laser pulse shape. The common optical fiducial serves as a reference for both the neutron signal and the laser pulse, thereby enabling accurate timing of the NTD signal.

A similar system to the one that images the OMEGA fiducial on the photocathode is used to image the light from a 2-GHz

comb generator onto the ROSS photocathode. The signal from this comb generator can be used to linearize the sweep speed of the streak camera.

Shielding Performance

Figure 145.37(a) shows the charge-coupled-device (CCD) image recorded by the P11-NTD diagnostics from a high-yield DT cryo shot (2.6×10^{13} neutrons). Four of the eight fiducial pulses are visible at the top of the image and six of the pulses from the 2-GHz comb generator are seen at the bottom. The CCD image shows very little background compared to the CCD image recorded with the previous-generation NTD system, called H5-NTD [see Fig. 145.38(a)], at the same yield level. The H5-NTD diagnostic also uses a ROSS streak camera, which is mounted ~ 3 m from the target in the Target Bay, shielded by 50 cm of CH in the direct line of sight and 10 cm of CH in all other directions. Figures 145.37(b) and 145.38(b) show the respective horizontal lineouts through the signals summed over the whole vertical width. Since the scintillator has a very fast rise time of <20 ps and a decay time of ~ 1.2 ns, the neutron-

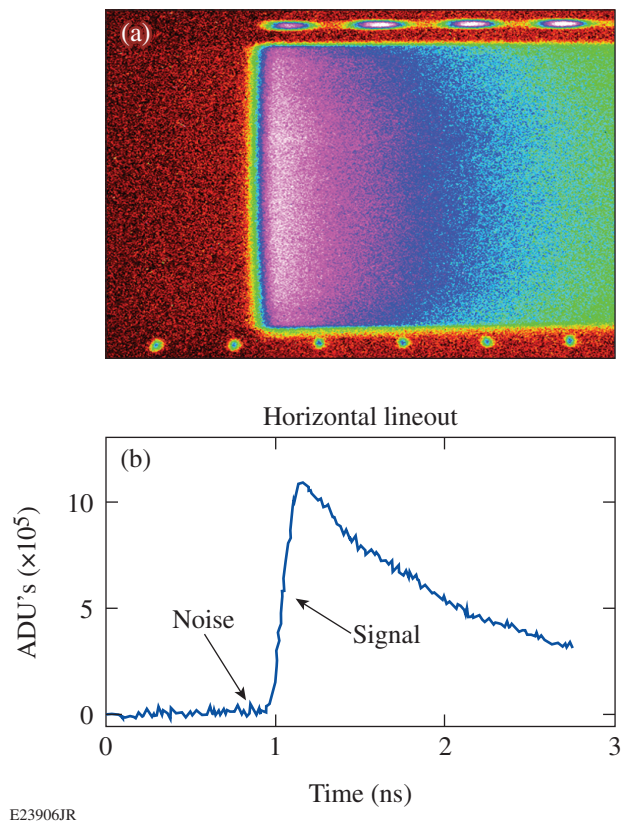


Figure 145.37

(a) A charge-coupled-device (CCD) image from P11-NTD from a high-yield DT cryo shot (2.6×10^{13} neutrons) and (b) a horizontal lineout through the signal summed over the whole vertical width in analog digital units (ADU's).

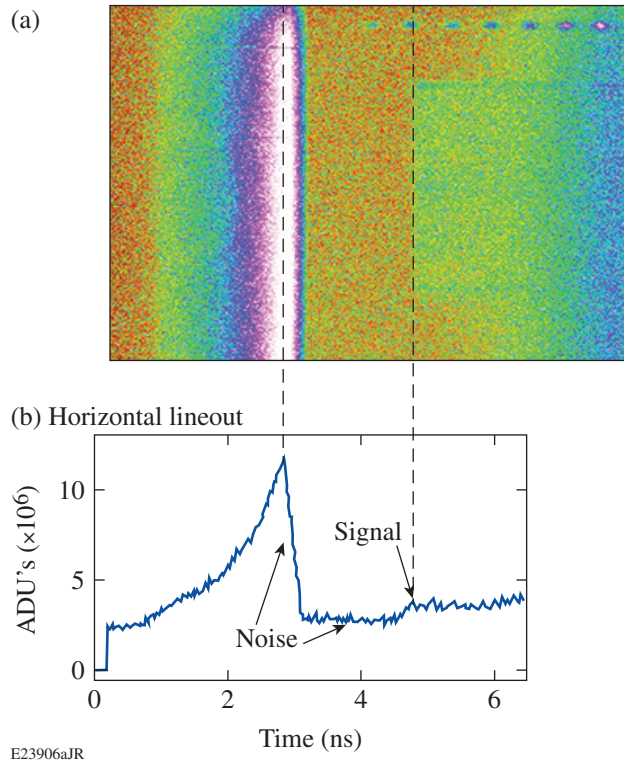


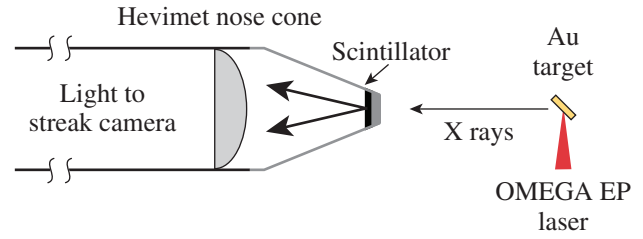
Figure 145.38

(a) A CCD image from H5-NTD from a high-yield DT cryo shot (2.6×10^{13} neutrons) and (b) horizontal lineout through the signal summed over the entire vertical width.

production history information is encoded in the leading edge of the pulse. The most-prominent feature of the background on the H5-NTD signal is a spike at ~ 2.5 ns, which is most likely caused by scattered neutron background present during the retrace of the streak, which starts a few microseconds after the sweep. The signal-to-noise on the P11-NTD system is ~ 50 , which is an $\sim 200\times$ improvement over H5-NTD with a signal-to-noise ratio of ~ 0.25 at this yield level. As expected, this improvement is less than the difference the line-of-sight shielding and solid angle ($10\times$ improvement resulting from distance) would indicate.

Impulse-Response Calibration

The impulse response of the full P11-NTD including the scintillator, optical transport, and streak camera was measured using x rays from a target illuminated by a short laser pulse (10 ps) from OMEGA EP (see Fig. 145.39). The shielding from the 2-mm-thick tungsten alloy nose cone allows only hard x rays (>200 keV) to interact with the scintillator. Hard x rays are a reasonable substitute for neutrons to generate light in the scintillator because they interact mostly via Compton scattering in the CH scintillator substrate, which generates fast electrons.



E9262JR

Figure 145.39

Setup of the calibration of the P11-NTD impulse response using x rays from an Au target illuminated by a short OMEGA EP laser pulse (10 ps). The 2-mm-thick Hevimet nose cone allows only hard x rays (>200 keV) to interact with the scintillator.

These >100 -keV electrons generate electron-hole pairs similar to the MeV protons produced by the elastic scattering from an incident neutron. Even though the electron-hole pair density for the fast electron is significantly lower than that for a proton because of the difference in stopping power, it is a better substitute for neutron interaction relative to the excitation of the scintillator by UV irradiation, which interacts mostly with the dyes in the scintillator.²⁵

For calibration, the OMEGA EP laser was defocused to spot sizes between 150 and 175 μm and the pulse energy was reduced to ~ 400 J to optimize the signal on the P11-NTD streak camera. The target was an Au foil of $500 \times 500 \times 10$ - μm size. Figure 145.40(a) shows the temporal history of the signal from four laser shots with different focal-spot conditions for a 3-ns streak-camera sweep window. This signal is obtained by removing the effect of the long scintillator decay from the recorded signal using a “physical-modeling” approach for the deconvolution.¹¹ The signal n_i at the pixel location i is given as the recorded signal s_i minus the sum of all earlier neutron signals, which decay exponentially at the scintillator fall time τ , with Δt_p as the time separation of two pixels:

$$n_i = s_i - \sum_{j=0}^{i-1} n_j \exp\left[-\frac{(i-j) \times \Delta t_p}{\tau}\right]. \quad (1)$$

The signals from the x-ray calibration show a stable center section of approximately Gaussian shape with a FWHM of $\sim 50 \pm 2$ ps, as well as a shoulder (at the start of the signal) and a tail, which both vary with focus condition [see Fig. 145.40(a)]. The shoulder ahead of the main pulse is most likely caused by Cherenkov radiation from MeV Compton-scattered electrons in the $f/2$ collection system since a MeV electron gains ~ 20 ps/cm on light in glass. The tail after the pulse could be from subrela-

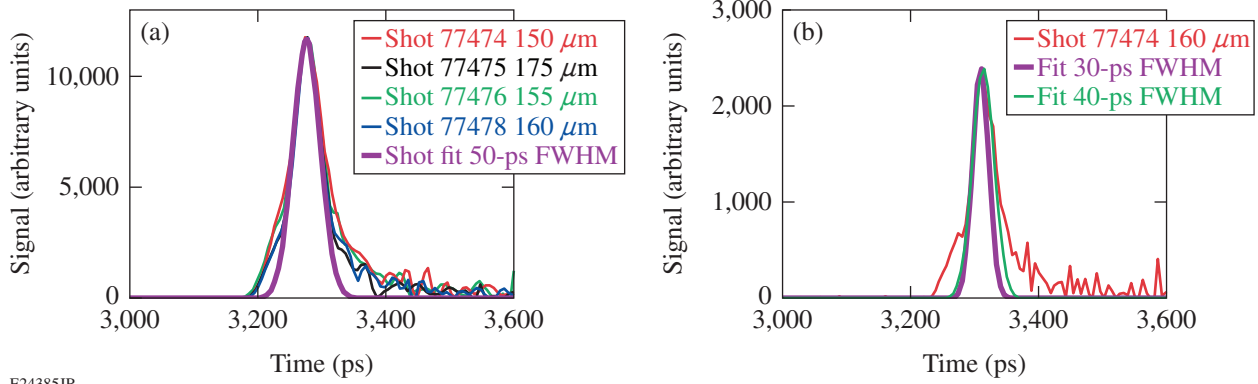


Figure 145.40

(a) Unfolded P11-NTD signals from the impulse response calibrations with a 3-ns sweep window at different focus conditions of the short-pulse laser. A 50-ps FWHM Gaussian fit matches the central part of the signal well. (b) Unfolded P11-NTD signals from the impulse response calibrations with a 1.5-ns sweep window; both a 30-ps and a 40-ps Gaussian are shown.

tivistic electrons generated in the laser–target interaction hitting the high-Z nose cone, generating hard x-ray bremsstrahlung. Both of these effects should scale with laser intensity since the slope of the electron energy distribution should be steeper for a lower laser intensity, which corresponds to a lower number of high- and medium-energy electrons.

A single shot was taken with a faster sweep speed corresponding to a 1.5-ns sweep window [see Fig. 145.40(b)]. Because of the degraded signal-to-noise, a stable fit of a Gaussian to the peak of the signal is no longer possible; several different fits with 30- to 40-ps FWHM are consistent with the data.

To infer the impulse response of the P11-NTD system, the width of the x-ray pulse must be subtracted. Since there is no independent measurement of the x-ray pulse duration, simple estimates must be used. A good estimate of the minimum x-ray pulse duration is ~ 15 ps because the laser pulse is ~ 10 ps long and the hot electrons generated in the laser–target interaction typically have a lifetime of a few picoseconds.²⁶ The maximum pulse duration cannot be longer than the shortest measured pulse duration with the 1.5-ns sweep of ~ 35 ps. Consequently, a reasonable estimate of the x-ray pulse duration is 25 ± 10 ps. Subtracting the x-ray pulse in quadrature from the measured FWHM of the signal yields an impulse response of $\sim 40 \pm 10$ ps for the 3-ns sweep window and $\sim 25 \pm 10$ ps for the 1.5-ns sweep window, respectively.

Data Analysis

Figure 145.41 shows the inferred neutron rate from the deconvolved P11-NTD signal recorded on a recent DT cryogenic implosion on OMEGA with a neutron yield of $\sim 4 \times 10^{13}$. The measured neutron temporal history is broadened by several

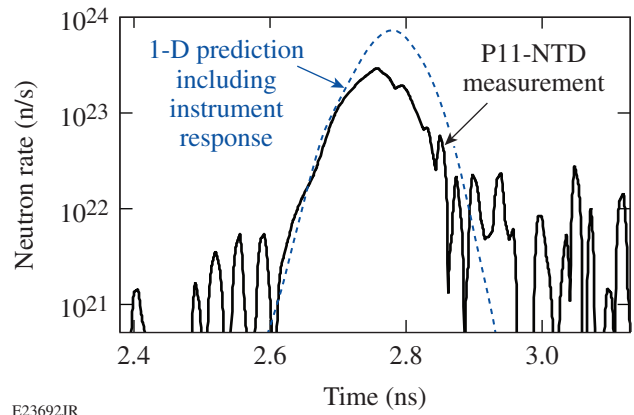


Figure 145.41

Unfolded P11-NTD signal from a high-yield cryo shot (neutron yield of $\sim 4 \times 10^{13}$), compared to results from 1-D LILAC hydro simulations.

different mechanisms, which must be subtracted to measure the actual width of the neutron pulse from the target. Broadening the neutron energy spectrum caused by the high temperature of the thermonuclear plasma leads to an arrival time spread in the scintillator for DT neutrons:¹⁰

$$\Delta t_T^{\text{DT}} = 122\sqrt{T} \times d, \quad (2)$$

where Δt_T^{DT} is the FWHM of the spread in picoseconds, d is the target-to-detector distance in meters, and T is the neutron-averaged ion temperature in keV. For a 10-cm distance of the P11-NTD scintillator to the target, this effect broadens the signal by ~ 25 ps at a 4-keV ion temperature, which is typical for most of the high-yield cryo implosions on OMEGA. Additionally, the finite neutron transit time through the scintil-

lator $\Delta t_s = \Delta x/v_n$ broadens the signal by $\Delta t_s^{DT} = 20$ ps for a scintillator thickness of $\Delta x = 1$ mm and a DT neutron speed of $v_n = 5.12$ cm/ns. Since the shape of the neutron rate is not far from a Gaussian, the impulse response of the instrument, the thermal broadening, and the transit time spread can be subtracted from the measured FWHM of the signal in quadrature to infer the actual neutron pulse width. For a measured FWHM of the neutron signal of 82 ± 2 ps, the resultant neutron pulse width is calculated to be 65 ± 6 ps.

An alternative method of interpreting the experimental data is to convolve the calculated neutron rate from a simulation with the experimental broadening and compare it to the measured signal. Figure 145.41 compares the results of a 1-D *LILAC* simulation of the cryogenic implosion¹⁷ convolved with the experimental broadening and the P11-NTD data. Since the absolute timing of the NTD instruments is typically of the order of 50 ps (Ref. 11), the simulation data were shifted by ~ 20 ps to better align with the rising edge of the experimental data. The simulation matches the experimental data very well on the rising edge over more than one order of magnitude in neutron rate. The experimental and simulated neutron rates start to deviate from each other close to the peak of the neutron pulse, with the experimental rate significantly lower than the simulation. This deviation is believed to be caused by 3-D effects, which mix cold material into the hot core plasma, quenching the neutron-production rate earlier than expected in the 1-D simulations.⁷

Summary and Outlook

A new neutron temporal diagnostic (P11-NTD) has been developed to measure the temporal history of the neutron production in high-yield, high-performance cryogenic DT implosions on OMEGA. The ROSS streak camera recording system was placed ~ 11 m from target chamber center behind the primary shield wall, which reduced the neutron background by a factor of ~ 200 . The remote location of the streak camera required the construction of a complex 16.2-m-long image relay to transport the light from the scintillator to the streak camera. The impulse response of the P11-NTD system was measured using hard x rays generated from the interaction of the 10-ps OMEGA EP laser pulse with an Au target. With the standard 3-ns sweep window an impulse response of $\sim 40 \pm 10$ ps was inferred, which makes it possible to measure ~ 65 -ps FWHM neutron pulses with an accuracy of $\sim 10\%$. Preliminary measurements of the impulse response of the system using a 1.5-ns sweep window showed an improved impulse response of $\sim 25 \pm 10$ ps, which would enable the P11-NTD to measure ~ 50 -ps FWHM neutron pulses with $\sim 10\%$ accuracy once this mode of operation is fully validated.

The technique of placing the streak camera of a NTD system outside the bioshield could be relatively easily adapted to larger ICF facilities like the National Ignition Facility (NIF)²⁷ or Laser Mégajoule (LMJ).²⁸ With a typical distance of the shield wall of ~ 15 m from the target, an NTD on these facilities would need an ~ 20 -m-long optical relay, which could be designed without compromising the temporal resolution. Given the much-higher neutron yields at the NIF or LMJ, the constraints on the optical transmission of the relay system are significantly relaxed and a narrowband (2- to 10-nm) optical filter at the peak of the scintillator emission spectrum could be used to minimize the chromatic group velocity dispersion.

ACKNOWLEDGMENT

This material is based upon work supported by the Department of Energy National Nuclear Security Administration under Award Number DE-NA0001944, the University of Rochester, and the New York State Energy Research and Development Authority. The support of DOE does not constitute an endorsement by DOE of the views expressed in this article.

REFERENCES:

1. J. H. Nuckolls, *Phys. Today* **35**, 24 (1982).
2. R. S. Craxton, K. S. Anderson, T. R. Boehly, V. N. Goncharov, D. R. Harding, J. P. Knauer, R. L. McCrory, P. W. McKenty, D. D. Meyerhofer, J. F. Myatt, A. J. Schmitt, J. D. Sethian, R. W. Short, S. Skupsky, W. Theobald, W. L. Kruer, K. Tanaka, R. Betti, T. J. B. Collins, J. A. Delettrez, S. X. Hu, J. A. Marozas, A. V. Maximov, D. T. Michel, P. B. Radha, S. P. Regan, T. C. Sangster, W. Seka, A. A. Solodov, J. M. Soures, C. Stoeckl, and J. D. Zuegel, *Phys. Plasmas* **22**, 110501 (2015).
3. O. A. Hurricane, D. A. Callahan, D. T. Casey, E. L. Dewald, T. R. Dittrich, T. Döppner, M. A. Barrios Garcia, D. E. Hinkel, L. F. Berzak Hopkins, P. Kervin, J. L. Kline, S. Le Pape, T. Ma, A. G. MacPhee, J. L. Milovich, J. Moody, A. E. Pak, P. K. Patel, H.-S. Park, B. A. Remington, H. F. Robey, J. D. Salmonson, P. T. Springer, R. Tommasini, L. R. Benedetti, J. A. Caggiano, P. Celliers, C. Cerjan, R. Dylla-Spears, D. Edgell, M. J. Edwards, D. Fittinghoff, G. P. Grim, N. Guler, N. Izumi, J. A. Frenje, M. Gatu Johnson, S. Haan, R. Hatarik, H. Herrmann, S. Khan, J. Knauer, B. J. Kozioziemski, A. L. Kritcher, G. Kyrala, S. A. Maclaren, F. E. Merrill, P. Michel, J. Ralph, J. S. Ross, J. R. Rygg, M. B. Schneider, B. K. Spears, K. Widmann, and C. B. Yeaman, *Phys. Plasmas* **21**, 056314 (2014).
4. M. R. Gomez *et al.*, *Phys. Plasmas* **22**, 056306 (2015).
5. J. A. Frenje, C. K. Li, F. H. Séguin, J. Deciantis, S. Kurebayashi, J. R. Rygg, R. D. Petrasso, J. Delettrez, V. Yu. Glebov, C. Stoeckl, F. J. Marshall, D. D. Meyerhofer, T. C. Sangster, V. A. Smalyuk, and J. M. Soures, *Phys. Plasmas* **11**, 2798 (2004).
6. I. V. Igumenshchev, W. Seka, D. H. Edgell, D. T. Michel, D. H. Froula, V. N. Goncharov, R. S. Craxton, L. Divol, R. Epstein, R. Follett, J. H. Kelly, T. Z. Kosc, A. V. Maximov, R. L. McCrory, D. D. Meyerhofer, P. Michel, J. F. Myatt, T. C. Sangster, A. Shvydky, S. Skupsky, and C. Stoeckl, *Phys. Plasmas* **19**, 056314 (2012).

7. P. B. Radha, T. J. B. Collins, J. A. Delettrez, Y. Elbaz, R. Epstein, V. Yu. Glebov, V. N. Goncharov, R. L. Keck, J. P. Knauer, J. A. Marozas, F. J. Marshall, R. L. McCrory, P. W. McKenty, D. D. Meyerhofer, S. P. Regan, T. C. Sangster, W. Seka, D. Shvarts, S. Skupsky, Y. Srebro, and C. Stoeckl, *Phys. Plasmas* **12**, 056307 (2005).
8. G. F. Knoll, *Radiation Detection and Measurement*, 4th ed. (John Wiley, Hoboken, NJ, 2010).
9. G. J. Schmid, R. L. Griffith, N. Izumi, J. A. Koch, R. A. Lerche, M. J. Moran, T. W. Phillips, R. E. Turner, V. Yu. Glebov, T. C. Sangster, and C. Stoeckl, *Rev. Sci. Instrum.* **74**, 1828 (2003).
10. R. A. Lerche, D. W. Phillion, and G. L. Tietbohl, *Rev. Sci. Instrum.* **66**, 933 (1995).
11. C. Stoeckl, V. Yu. Glebov, S. Roberts, T. C. Sangster, R. A. Lerche, R. L. Griffith, and C. Sorce, *Rev. Sci. Instrum.* **74**, 1713 (2003).
12. R. A. Lerche *et al.*, *Rev. Sci. Instrum.* **59**, 1697 (1988).
13. J-P. Garçonnet *et al.*, *Rev. Sci. Instrum.* **63**, 4871 (1992).
14. C. Stoeckl, V. Yu. Glebov, J. D. Zuegel, D. D. Meyerhofer, and R. A. Lerche, *Rev. Sci. Instrum.* **73**, 3796 (2002).
15. V. Yu. Glebov, D. D. Meyerhofer, T. C. Sangster, C. Stoeckl, S. Roberts, C. A. Barrera, J. R. Celeste, C. J. Cerjan, L. S. Dauffy, D. C. Eder, R. L. Griffith, S. W. Haan, B. A. Hammel, S. P. Hatchett, N. Izumi, J. R. Kimbrough, J. A. Koch, O. L. Landen, R. A. Lerche, B. J. MacGowan, M. J. Moran, E. W. Ng, T. W. Phillips, P. M. Song, R. Tommasini, B. K. Young, S. E. Caldwell, G. P. Grim, S. C. Evans, J. M. Mack, T. Sedillo, M. D. Wilke, D. C. Wilson, C. S. Young, D. Casey, J. A. Frenje, C. K. Li, R. D. Petrasso, F. H. Séguin, J. L. Bourgade, L. Disdier, M. Houry, I. Lantuejoul, O. Landoas, G. A. Chandler, G. W. Cooper, R. J. Lepeér, R. E. Olson, C. L. Ruiz, M. A. Sweeney, S. P. Padalino, C. Horsfield, and B. A. Davis, *Rev. Sci. Instrum.* **77**, 10E715 (2006).
16. Q. Tang *et al.*, *Rev. Sci. Instrum.* **85**, 046108 (2014).
17. V. N. Goncharov, T. C. Sangster, R. Betti, T. R. Boehly, M. J. Bonino, T. J. B. Collins, R. S. Craxton, J. A. Delettrez, D. H. Edgell, R. Epstein, R. K. Follet, C. J. Forrest, D. H. Froula, V. Yu. Glebov, D. R. Harding, R. J. Henchen, S. X. Hu, I. V. Igumenshev, R. Janezic, J. H. Kelly, T. J. Kessler, T. Z. Kosc, S. J. Loucks, J. A. Marozas, F. J. Marshall, A. V. Maximov, R. L. McCrory, P. W. McKenty, D. D. Meyerhofer, D. T. Michel, J. F. Myatt, R. Nora, P. B. Radha, S. P. Regan, W. Seka, W. T. Shmayda, R. W. Short, A. Shvydky, S. Skupsky, C. Stoeckl, B. Yaakobi, J. A. Frenje, M. Gatu-Johnson, R. D. Petrasso, and D. T. Casey, *Phys. Plasmas* **21**, 056315 (2014).
18. T. R. Boehly, D. L. Brown, R. S. Craxton, R. L. Keck, J. P. Knauer, J. H. Kelly, T. J. Kessler, S. A. Kumpan, S. J. Loucks, S. A. Letzring, F. J. Marshall, R. L. McCrory, S. F. B. Morse, W. Seka, J. M. Soures, and C. P. Verdon, *Opt. Commun.* **133**, 495 (1997).
19. Saint-Gobain Crystals, Newbury, OH 44065 (see <http://www.crystals.saint-gobain.com/>).
20. R. A. Lerche *et al.*, *Rev. Sci. Instrum.* **75**, 4042 (2004).
21. C. Stoeckl, M. Cruz, V. Yu. Glebov, J. P. Knauer, R. Lauck, K. Marshall, C. Mileham, T. C. Sangster, and W. Theobald, *Rev. Sci. Instrum.* **81**, 10D302 (2010).
22. C. Stoeckl, J. A. Delettrez, J. H. Kelly, T. J. Kessler, B. E. Kruschwitz, S. J. Loucks, R. L. McCrory, D. D. Meyerhofer, D. N. Maywar, S. F. B. Morse, J. Myatt, A. L. Rigatti, L. J. Waxer, J. D. Zuegel, and R. B. Stephens, *Fusion Sci. Technol.* **49**, 367 (2006).
23. Schott North America, Inc., Elmsford, NY 10523 (see <http://www.us.schott.com>).
24. W. R. Donaldson, R. Boni, R. L. Keck, and P. A. Jaanimagi, *Rev. Sci. Instrum.* **73**, 2606 (2002).
25. Y. Arikawa *et al.*, *2007 Annual Progress Report*, 47, Institute for Laser Engineering, Osaka University, Osaka, Japan (February 2008).
26. W. Theobald, A. A. Solodov, C. Stoeckl, K. S. Anderson, F. N. Beg, R. Epstein, G. Fiksel, E. M. Giraldez, V. Yu. Glebov, H. Habara, S. Ivancic, L. C. Jarrott, F. J. Marshall, G. McKiernan, H. S. McLean, C. Mileham, P. M. Nilson, P. K. Patel, F. Pérez, T. C. Sangster, J. J. Santos, H. Sawada, A. Shvydky, R. B. Stephens, and M. S. Wei, *Nat. Commun.* **5**, 5785 (2014).
27. J. D. Lindl and E. I. Moses, *Phys. Plasmas* **18**, 050901 (2011).
28. D. Besnard, *J. Phys.: Conf. Ser.* **112**, 012004 (2008).